Chapter 7

Spatial $\mathcal{H}_2$ control

In this chapter, we discuss the controller design procedure that is based on the spatial $\mathcal{H}_2$ norm concept discussed in Chapter 3. This spatial $\mathcal{H}_2$ controller can be viewed as a natural extension of the standard $\mathcal{H}_2$ controller for spatially distributed systems. In this case, the spatial information conveyed in the system is incorporated in the controller design. Here, we extend the spatial $\mathcal{H}_2$ control concept to smart structure systems. We will design and implement the spatial $\mathcal{H}_2$ controller on a piezoelectric laminate beam [HM01a, HM02c].

The controller will be designed such that the spatial $\mathcal{H}_2$ norm of the closed-loop system is minimized. This optimization procedure will guarantee vibration suppression over the entire structure in a spatially-averaged sense. To solve for the optimization, the spatial $\mathcal{H}_2$ control problem can be formulated as a standard $\mathcal{H}_2$ control optimization problem. This allows a standard optimization methodology to be used to obtain our spatial $\mathcal{H}_2$ controller. We will demonstrate the effectiveness of the spatial $\mathcal{H}_2$ controller in suppressing vibration of the first six flexural modes of a piezoelectric laminate beam.

7.1 Spatial $\mathcal{H}_2$ control of flexible structures

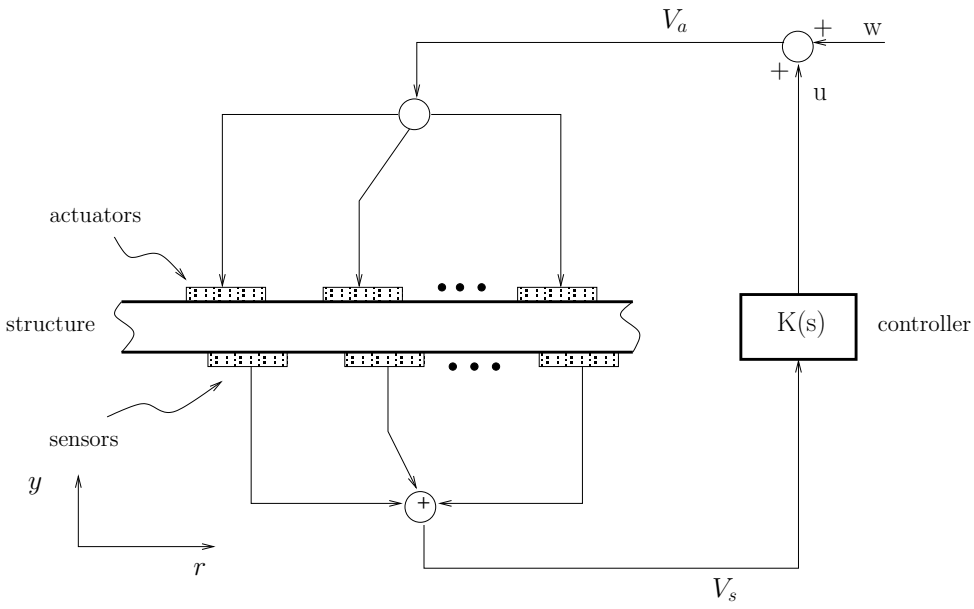

Figure 7.1: Control of flexible structures

Consider the flexible structure in Figure 7.1, where the actuators and sensors used are assumed to be piezoelectric transducers bonded to the structure. However, the actuators and sensors are not necessarily collocated. A state-space representation of such a spatially distributed LTI dynamical system is

$$\begin{aligned} \dot{\bar{x}}(t) &= A\bar{x}(t) + B_1 w(t) + B_2 u(t) \\ y(t,r) &= C_1(r)\bar{x}(t) + D_{11}(r)w(t) + D_{12}(r)u(t) \\ V_s(t) &= C_2\bar{x}(t) + D_{21}w(t) + D_{22}u(t) \end{aligned} \tag{7.1}$$

where $\bar{x} \in \mathbf{R}^q$ contains the states, $w \in \mathbf{R}^m$ is the disturbance input, $u \in \mathbf{R}^m$ is the control input, $V_s \in \mathbf{R}^n$ is the measured output, $y \in \mathbf{R} \times \mathcal{R}$ is the performance output and $r \in \mathcal{R}$. For a flexible structure, y represents the spatial displacement at time t at location r. The controller is designed to reduce the effect of disturbance w on the entire structure. Here, the disturbance w is assumed to enter through the actuator channels, i.e. $D_{22} = D_{21}, D_{11}(r) = D_{12}(r)$

and $B_1 = B_2$. However, a general case of disturbance can be dealt with in a similar manner.

The feedthrough terms in (7.1) may be important for compensating for the truncation error in the model as discussed in Chapter 4. This yields a system that is not strictly proper, which can cause difficulties since the spatial $\mathcal{H}_2$ norm of the system has to be finite. To overcome this problem, we replace the feedthrough terms in the performance output y (7.1) with a second-order out-of-bandwidth term similar to that in Chapter 6. Typically for the above problem, the second-order term has the form:

$$\frac{\alpha_c(r)}{s^2 + 2\zeta_c\omega_c s + \omega_c^2}$$

where

$$\frac{\alpha_c(r)}{\omega_c^2} \;=\; D_{11}(r) \;=\; D_{12}(r). \tag{7.2}$$

Incorporating the second-order term into the original system, we obtain

$$\begin{aligned} \dot{\tilde{x}}(t) &= \tilde{A}\tilde{x}(t) + \tilde{B}_1 w(t) + \tilde{B}_2 u(t) \\ y(t,r) &= \tilde{C}_1(r)\tilde{x}(t) \\ V_s(t) &= \tilde{C}_2\tilde{x}(t) + D_{21}w(t) + D_{22}u(t) \end{aligned} \tag{7.3}$$

where $\tilde{x}$ consists of the original states of the plant $\bar{x}$ and the states due to the extra second-order term.

The spatial $\mathcal{H}_2$ control problem is to design a controller

$$\begin{aligned} \dot{x}_k(t) &= A_k x_k(t) + B_k V_s(t) \\ u(t) &= C_k x_k(t) + D_k V_s(t) \end{aligned} \tag{7.4}$$

such that the weighted spatial $\mathcal{H}_2$ norm of the closed-loop system

$$\ll T_{yw}(s,r) \gg^2_{2,Q} \;=\; \frac{1}{2\pi}\int_{-\infty}^{\infty}\int_{\mathcal{R}} \mathrm{tr}\{T_{yw}(j\omega,r)^* Q(r) T_{yw}(j\omega,r)\} dr d\omega \quad (7.5)$$

is minimized. Here, $Q(r)$ is a spatial weighting function and T_{yw} is the closed-loop transfer function from w to y. $Q(r)$ can be used for emphasizing the region where the vibration reduction is to be more concentrated.

From Theorem 3.1, the above control problem can be transformed into a standard $\mathcal{H}_2$ control problem with the system:

$$\begin{aligned} \dot{\tilde{x}}(t) &= \tilde{A}\tilde{x}(t) + \tilde{B}_1 w(t) + \tilde{B}_2 u(t) \\ \tilde{y}(t) &= \Gamma\, \tilde{x}(t) \\ V_s(t) &= \tilde{C}_2\tilde{x}(t) + D_{21} w(t) + D_{22} u(t) \end{aligned} \quad (7.6)$$

where again $D_{21} = D_{22}$ and Γ is any matrix that satisfies

$$\Gamma^T\Gamma = \int_{\mathcal{R}} \tilde{C}_1(r)^T\, \tilde{C}_1(r)\, dr. \quad (7.7)$$

In practice, it might be necessary to include a control weight on the control signal to avoid an excessive controller gain. Excessive gain may lead to reduction of closed-loop robustness as well as other problems such as actuator saturation and noise sensitivity. This issue is addressed by extending the previous system (7.6) to include a weight factor R on the control signal:

$$\begin{aligned} \dot{\tilde{x}}(t) &= \tilde{A}\tilde{x}(t) + \tilde{B}_1 w(t) + \tilde{B}_2 u(t) \\ \hat{y}(t) &= \begin{bmatrix} \Gamma \\ 0 \end{bmatrix} \tilde{x}(t) + \begin{bmatrix} 0 \\ R \end{bmatrix} u(t) \\ V_s(t) &= \tilde{C}_2\tilde{x}(t) + D_{21} w(t) + D_{22} u(t). \end{aligned} \quad (7.8)$$

A compromise has to be made between the level of vibration reduction and controller gain by choosing a suitable R.

7.2 Spatial $\mathcal{H}_2$ control of a piezoelectric laminate beam

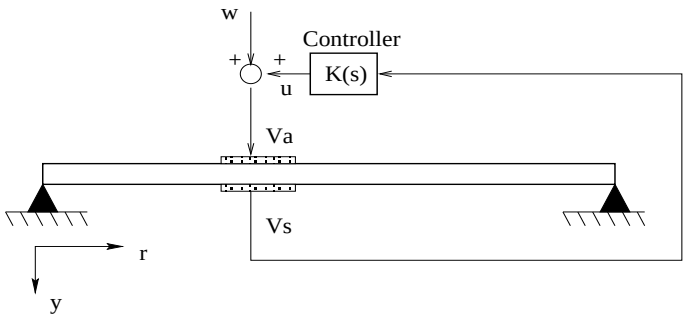

Figure 7.2: Control of a flexible beam

We consider a particular application of the spatial $\mathcal{H}_2$ control to a simply-supported beam with a collocated piezoelectric actuator/sensor pair (Figure 7.2). All the properties of the beam are similar to those described in Chapter 6 and can be seen in Table 4.2.

We concentrate on controlling the first six flexural modes of the beam. The model from modal analysis is truncated to include the first six modes to obtain a controller with a minimal order. Model correction is employed to compensate for the truncation error as discussed in Chapter 4. Here, we consider the truncated versions of G_{V_s} (2.89) and G (2.83). The corrected models are

$$\hat{G}_{Vs}(s) \;=\; \sum_{i=1}^{N} \frac{\Upsilon_i P_i}{s^2 + 2\zeta_i \omega_i s + \omega_i^2} + K_{V_s} \tag{7.9}$$

where $\Upsilon_i = \Omega_1 \Psi_{i1}, P_i = K_1 \Psi_{i1}$ and

$$\hat{G}_r(s,r) \;=\; \sum_{i=1}^{N} \frac{\phi_i(r)\, P_i}{s^2 + 2\zeta_i \omega_i s + \omega_i^2} + \sum_{i=N+1}^{N_a} K_{ri}^{opt} \phi_i(r). \tag{7.10}$$

Here, $N = 6$ since we wish to find a controller of minimal order to control the first six modes of the structure. Since the disturbance is assumed to enter the system through the same channel as the controller, the transfer function from w and u to the beam deflection y is $\hat{G}_r$ (7.10). Moreover, the transfer function from w and u to the collocated sensor voltage V_s is $\hat{G}_{Vs}$ (7.9).

We determine the feedthrough term in (7.9) from the experimental frequency-response data. The value of $D_{21} = D_{22} = K_{V_s}$ is found to be 0.033 if the first six modes are considered in the model. The feedthrough term is calculated based on modes $N+1$ to $N_a = 200$ to obtain a sufficient approximation to the feedthrough term. Here, we use the optimal feedthrough term that is based on the spatial $\mathcal{H}_2$ approach (4.16):

$$K_{ri}^{opt} = \frac{1}{2\omega_{co}\omega_i} \ln\left(\frac{\omega_i + \omega_{co}}{\omega_i - \omega_{co}}\right) P_i \tag{7.11}$$

where we assume the damping in the system is small and $\omega_{co} \in (\omega_N, \omega_{N+1}) =$ 795.8 Hz. To incorporate this feedthrough term into the system, we add a second-order term into the system as explained previously with $\zeta_c = 0.7$ and $\omega_c = 1.91$ KHz.

Hence, the system in (7.3) can be obtained with

$$\tilde{A} = \begin{bmatrix} 0_{(N+1)\times(N+1)} & I_{(N+1)\times(N+1)} \\ \tilde{A}_{1_{(N+1)\times(N+1)}} & \tilde{A}_{2_{(N+1)\times(N+1)}} \end{bmatrix}$$

where dimensions of each matrix are described above and

$$\begin{aligned} \tilde{A}_1 &= -\text{diag}(\omega_1^2 \ldots \omega_N^2 \;\; \omega_c^2) \\ \tilde{A}_2 &= -2\,\text{diag}(\zeta_1\omega_1 \ldots \zeta_N\omega_N \;\; \zeta_c\omega_c). \end{aligned}$$

Further,

$$\begin{aligned} \tilde{B}_1 = \tilde{B}_2 &= [0 \cdots 0 \;\; 0 \;\; K_1\Psi_{11} \cdots K_1\Psi_{N1} \;\; 1]^T \\ \tilde{C}_1(r) &= \left[\phi_1(r) \cdots \phi_N(r) \;\; \omega_c^2 \sum_{i=N+1}^{N_a} K_{ri}^{opt}\phi_i(r) \;\; 0 \cdots 0 \;\; 0\right] \\ \tilde{C}_2 &= \Omega_1 \left[\Psi_{11} \cdots \Psi_{N1} \;\; 0 \;\; 0 \cdots 0 \;\; 0\right] \\ D_{21} &= D_{22} = K_{V_s} = 0.033. \end{aligned} \tag{7.12}$$

In this particular application, $Q(r) = 1$ since the entire beam is weighted equally. Based on (7.7), the orthogonality property of the eigenfunctions ϕ_i (3.6) can be used to calculate Γ for the performance output $\hat{y}$ in (7.8):

$$\Gamma = \begin{bmatrix} \tilde{\Gamma}_{(N+1)\times(N+1)} & 0_{(N+1)\times(N+1)} \\ 0_{(N+1)\times(N+1)} & 0_{(N+1)\times(N+1)} \end{bmatrix} \tag{7.13}$$

where $\tilde{\Gamma} = \text{diag}\left(1 \ldots 1 \;\; \omega_c^2 \left(\Sigma_{i=N+1}^{N_a} (K_{ri}^{opt})^2\right)^{\frac{1}{2}}\right)$.

An equivalent standard $\mathcal{H}_2$ control problem (7.8) is then used to determine the optimal spatial $\mathcal{H}_2$ controller. Here, V_s is the output voltage from the piezoelectric sensor, while u is the control input voltage applied to the actuating patch. Matlab μ-Analysis and Synthesis Toolbox was used to calculate our spatial $\mathcal{H}_2$ controller.

7.3 Experimental implementation

The experimental set-up is similar to that in Chapter 6 and depicted in Figure 6.8. The apparatus was mounted on an optical table as shown in Figure 6.9. The sampling frequency was set at 20 KHz, while the cut-off frequencies of the two low-pass filters were set at 3 KHz.

The controller frequency response is shown in Figure 7.3. As expected, the controller has a resonant nature because of the highly resonant nature of the system. Figures 7.4 and 7.5 compare frequency responses of the open-loop and closed-loop systems (actuator voltage to sensor voltage) for both simulation and experimental results. The simulation and experimental results are reasonably close. The results demonstrate that our model is sufficiently accurate. It can be seen that the resonant responses of the first six modes are reduced by the controller action.

The robustness properties of the resulting closed-loop system are demonstrated in the following figures. Figures 7.6 and 7.7 compare the loop gain up to 1.6 KHz from simulation and experiment. Our simulation gives a gain margin of 12.4 dB at 1.55 KHz and a phase margin of 88.4^o at 78.5 Hz. The experiment gives a gain margin of 15.7 dB at 1.22 KHz, and a phase margin of 87.0^o at 79.1 Hz. The simulation prediction is reasonably close for the phase margin.

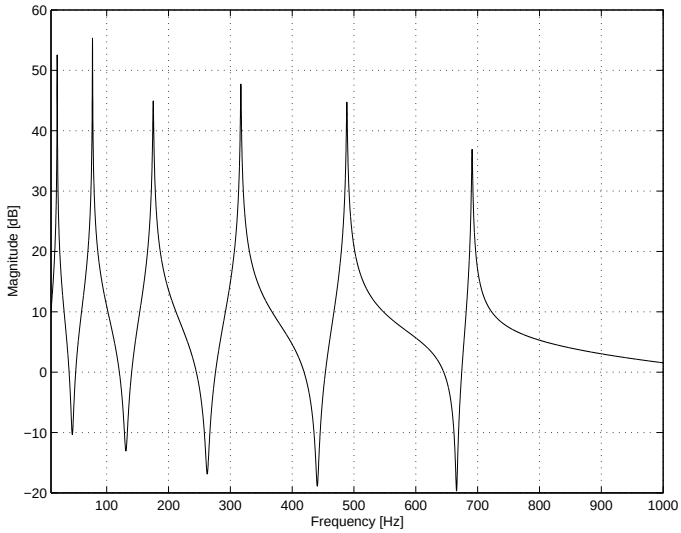

(a) magnitude

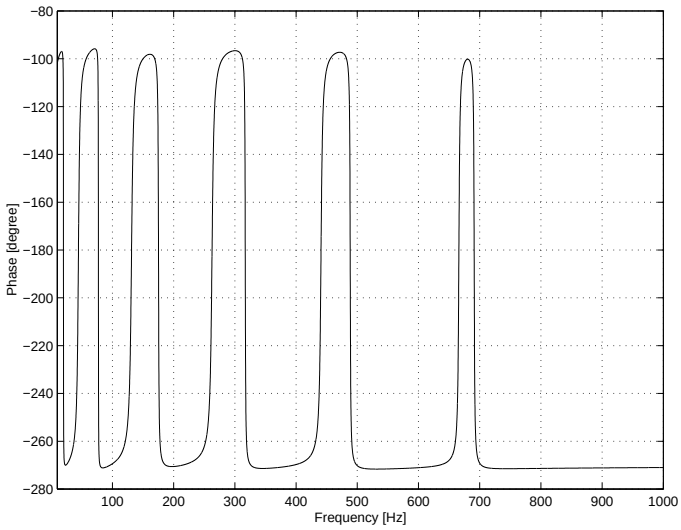

(b) phase

Figure 7.3: The frequency response of the controller (input voltage to output voltage [V/V])

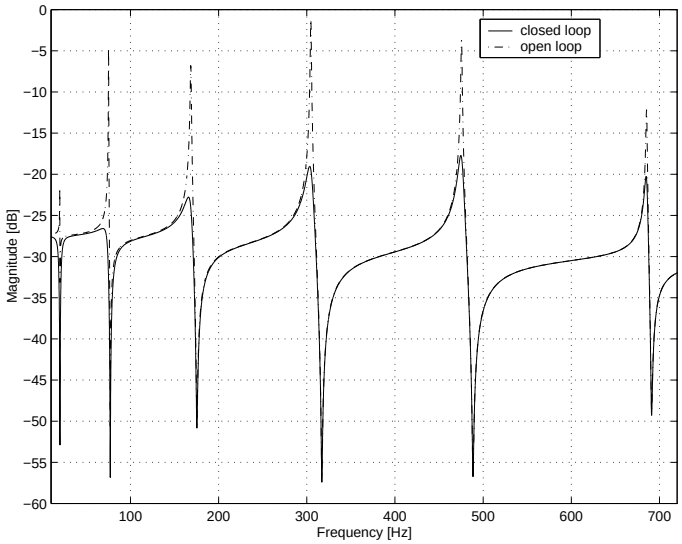

(a) simulation

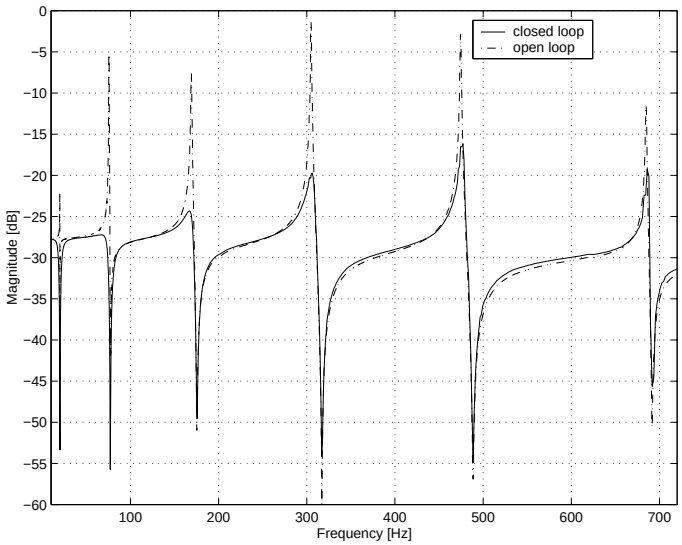

(b) experiment

Figure 7.4: Simulation and experimental frequency responses (actuator voltage to sensor voltage [V/V]) (magnitude)

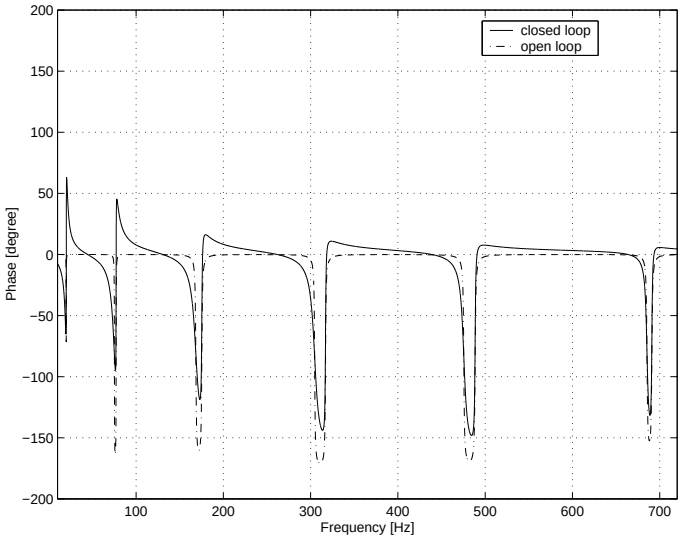

(a) simulation

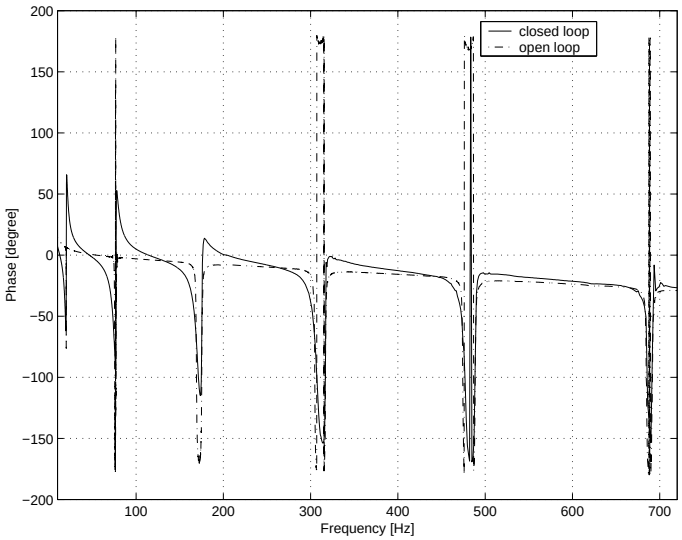

(b) experiment

Figure 7.5: Simulation and experimental frequency responses (actuator voltage to sensor voltage [V/V]) (phase)

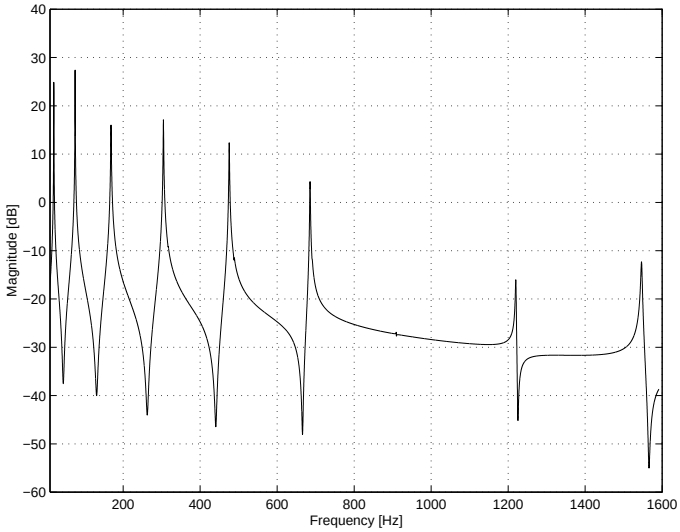

(a) simulation

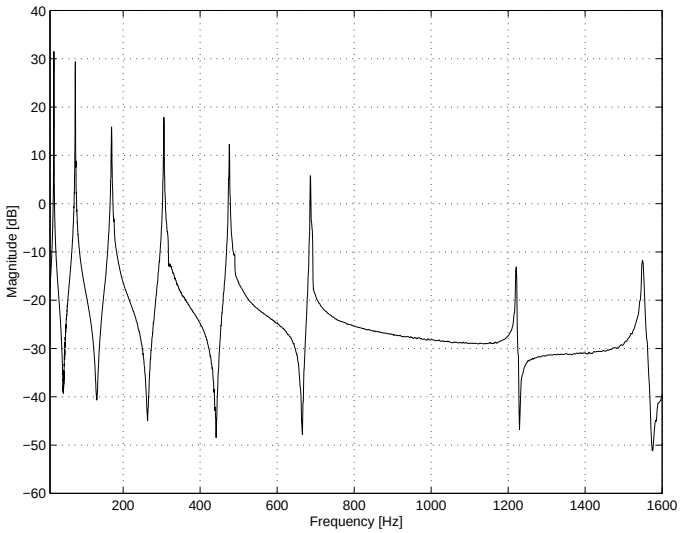

(b) experiment

Figure 7.6: Loop gain [V/V]: simulation and experiment (magnitude)

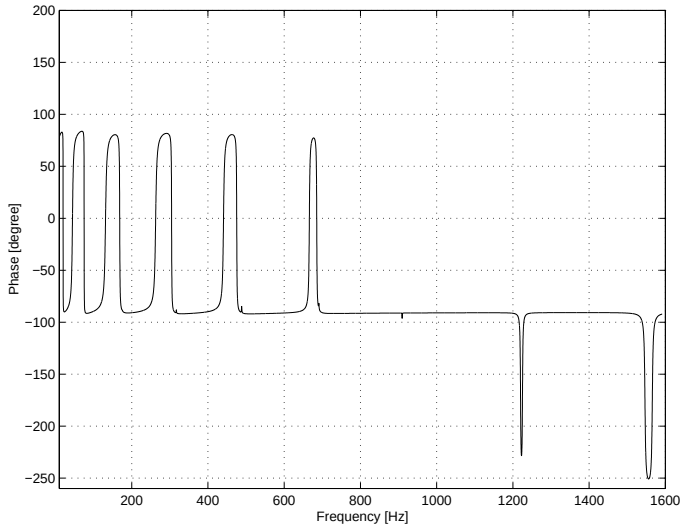

(a) simulation

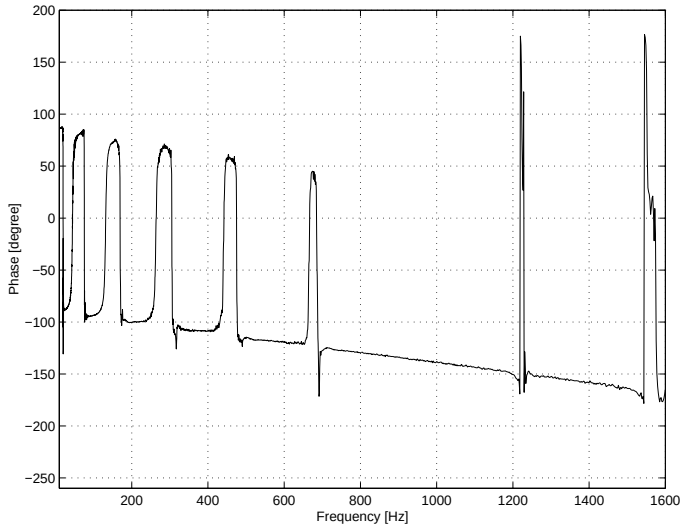

(b) experiment

Figure 7.7: Loop gain [V/V]: simulation and experiment (phase)

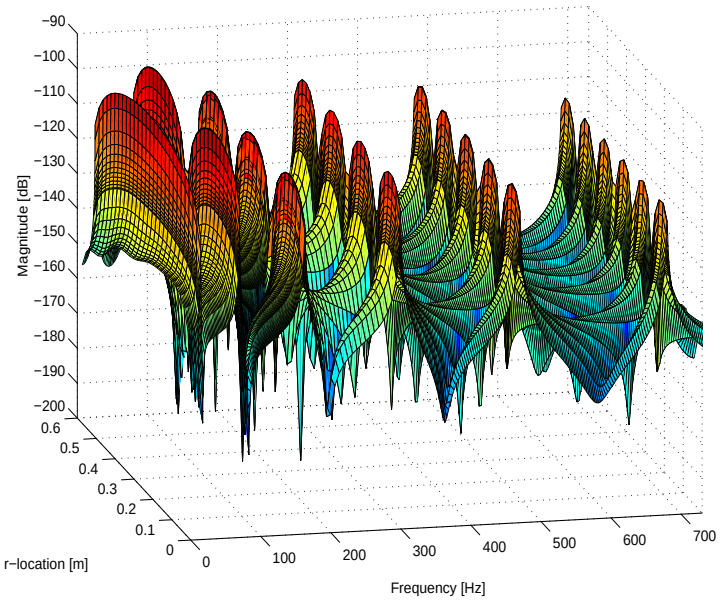

Figure 7.8: The simulated spatial frequency response: actuator voltage to beam deflection [m/V] (open loop)

However, there is a phase delay introduced by the digital implementation and filtering of the controller. This contributes to differences in the gain margin. In general, the controller has sufficient stability margins to ensure the robustness of the closed-loop system.

Figures 7.8 and 7.9 show the simulated spatial frequency responses of the uncontrolled and controlled beam respectively. The experimental spatial frequency responses of the uncontrolled beam are shown in Figure 7.10, while the controlled beam is shown in Figure 7.11. It is observed that the resonant responses of the first six modes have been reduced over the entire beam due to the controller action, which is as expected from the simulation (compare with Figures 7.8 and 7.9). The resonant responses of modes $1-6$ have been reduced by approximately $25.5, 28.5, 18, 18, 14$ and 7 dB respectively over the entire beam.

It may be asked what advantages the spatial $\mathcal{H}_2$ control has over the standard $\mathcal{H}_2$ control for spatially distributed systems. To answer this question, we need

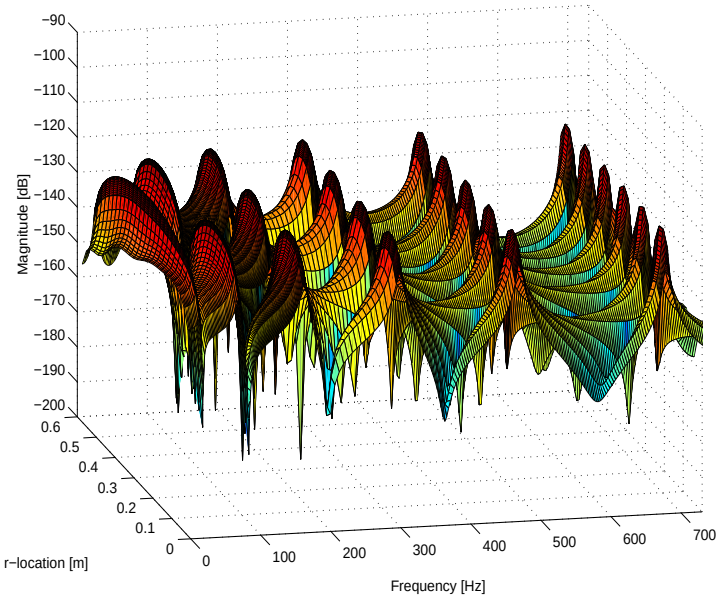

Figure 7.9: The simulated spatial frequency response: actuator voltage to beam deflection [m/V] (closed loop)

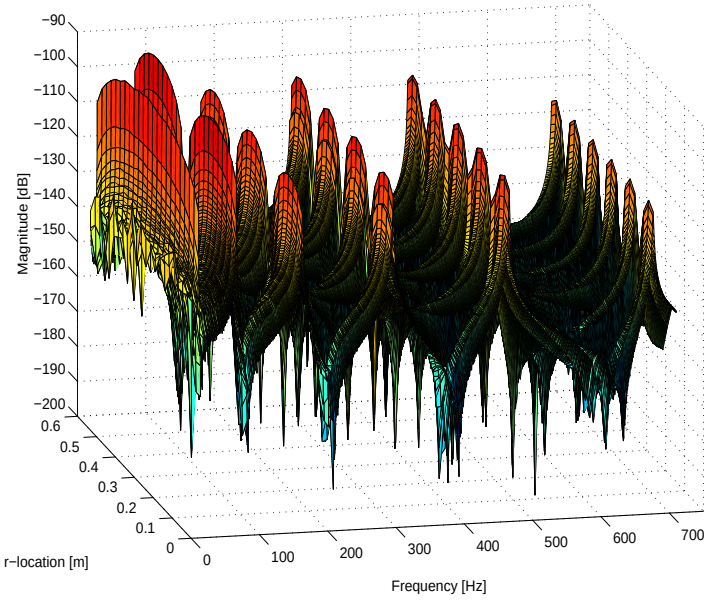

Figure 7.10: The experimental spatial frequency response: actuator voltage to beam deflection [m/V] (open loop)

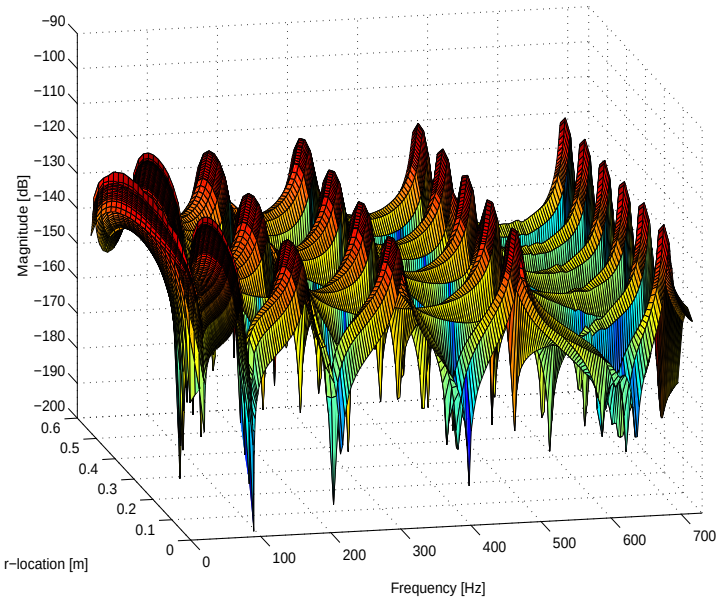

Figure 7.11: The experimental spatial frequency response: actuator voltage to beam deflection [m/V] (closed loop)

to compare the performance of both control methods in achieving vibration reduction for such systems. Based on our spatial $\mathcal{H}_2$ controller, we plotted the simulated $\mathcal{H}_2$ norm of the controlled and uncontrolled beam as a function of r in Figure 7.12 (a).

For a standard $\mathcal{H}_2$ control, the performance output y in (7.3) may imply a structural deflection at a particular location r along the beam. This corresponds to a pointwise $\mathcal{H}_2$ control since the controller minimizes the closed-loop transfer function from w to y at a specific point on the beam (at location r). Therefore, we designed a pointwise $\mathcal{H}_2$ controller by considering a particular location along the beam, e.g. y at the middle of the beam with $r = 0.3$ m. The gain and phase margins of the controller were 12.7 dB and 87.6^o respectively. Based on this pointwise controller, we also plotted $\mathcal{H}_2$ norm of the controlled and uncontrolled beam as a function of r in Figure 7.12 (b).

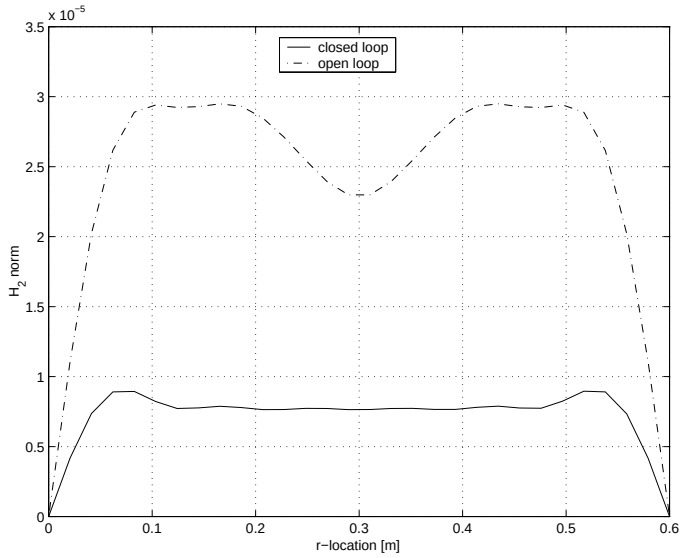

(a) spatial control

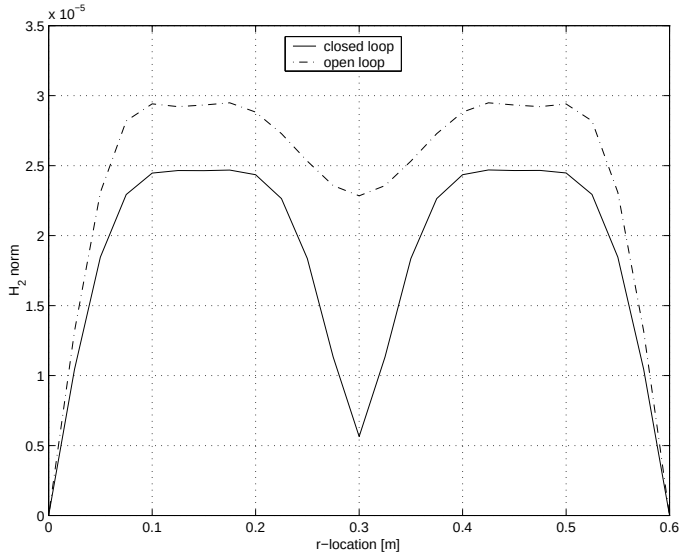

(b) pointwise control

Figure 7.12: Simulated $\mathcal{H}_2$ norm plots

Figure 7.12 (a) clearly demonstrates the effect of our spatial $\mathcal{H}_2$ controller in reducing the beam vibration. It is obvious that the $\mathcal{H}_2$ norm of the entire beam has been reduced in a more uniform manner. The highest $\mathcal{H}_2$ norm of the uncontrolled beam has been reduced by approximately 69.5%, from 2.95×10^{-5} to 9.0×10^{-6}.

Meanwhile, Figure 7.12 (b) shows the effectiveness of the pointwise control in local reduction of the $\mathcal{H}_2$ norm, especially at and around $r = 0.3$ m. This is as expected since the purpose of this controller is to minimize vibration at $r = 0.3$ m. In fact, the pointwise controller only suppresses the odd numbered modes since $r = 0.3$ m is a node for even numbered modes (for a simply-supported beam). Comparing Figures 7.12 (a) and (b), it can be concluded that the spatial $\mathcal{H}_2$ controller has an advantage over the pointwise $\mathcal{H}_2$ controller as it minimizes the vibration throughout the entire structure.

However, the standard $\mathcal{H}_2$ control can be designed to perform better spatially. This can be done by considering more points on the beam in the control design. For this particular case, the performance output will be a vector consisting of deflections y at several locations. However, this approach would lead to a rather complicated control design problem. Based on our observation, the spatial $\mathcal{H}_2$ control methodology provides a more natural way of including the spatial information in the system.

Figure 7.13 shows the effectiveness of the controller in minimizing beam vibration in time domain. A pulse signal of 100 V with duration of 15 s was applied through the piezoelectric actuator. The velocity response at the middle of the beam was observed using the PSV Laser Vibrometer. The velocity response was filtered by a low-pass filter with a cut-off frequency of 750 Hz. The settling time of the velocity response has been reduced by about 7 times due to controller action.

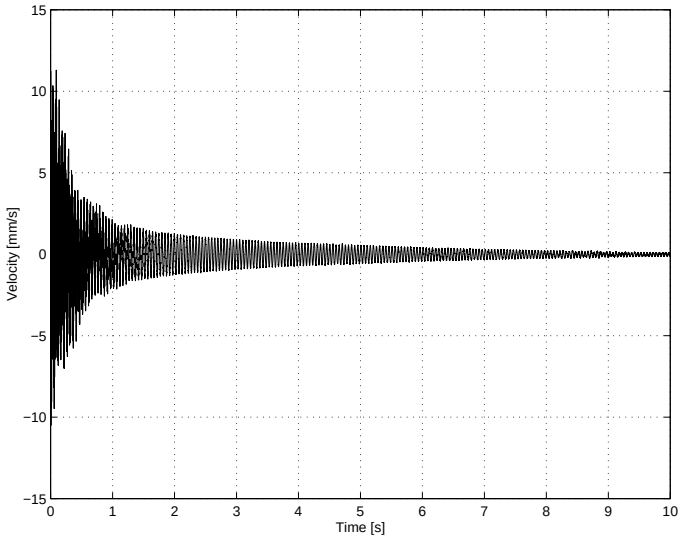

(a) open loop

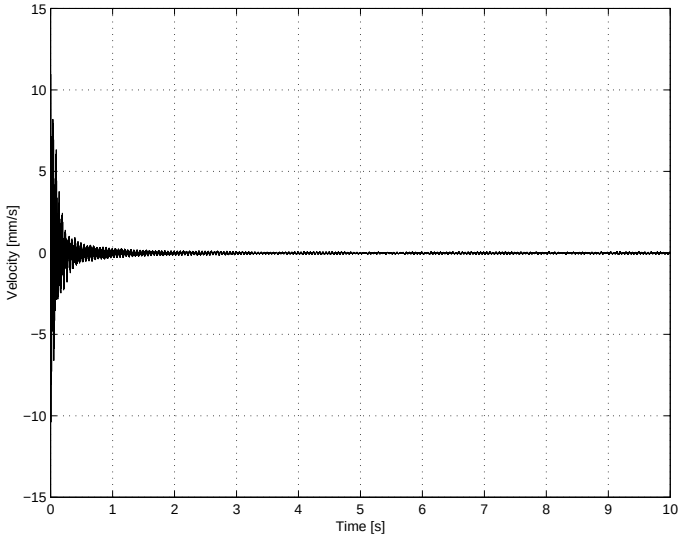

(b) closed loop

Figure 7.13: Vibration at the middle of the beam

7.4 Summary

We extended the spatial $\mathcal{H}_2$ norm concept for vibration control of smart structures. In particular, we designed and implemented a spatial $\mathcal{H}_2$ controller to minimize vibration of a piezoelectric laminate beam. The experiments demonstrated the effectiveness of the controller in minimizing structural vibration. We showed that the spatial $\mathcal{H}_2$ control has an advantage over the pointwise $\mathcal{H}_2$ control in minimizing the $\mathcal{H}_2$ norm across the structure. The methodology allows a design for control of spatially distributed systems that is more convenient than that of the standard $\mathcal{H}_2$ control.